

Photodissociation as a probe of the H_3^+ avoided crossing seam

Xavier Urbain,^{1,*} Arnaud Dochain,¹ Raphaël Marion,¹ Thibaut Launoy,^{1,2} and Jérôme Loreau^{1,2}

¹*Institute of Condensed Matter and Nanosciences, Université catholique de Louvain,
2 Chemin du Cyclotron, 1348, Louvain-la-Neuve, Belgium*

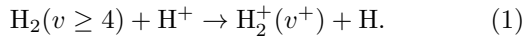
²*Laboratoire de Chimie Quantique et Photophysique, Université libre de Bruxelles,
50 av. F.D. Roosevelt, CP160/09, 1050 Brussels, Belgium*

Experiments are conducted to investigate the role of the avoided crossing seam in the photodissociation of H_3^+ . Three-dimensional imaging of dissociation products is used to determine the kinetic energy release and branching ratio among the fragmentation channels. Vibrational distributions are measured by dissociative charge transfer of H_2^+ products. It is found that the photodissociation of hot H_3^+ in the near ultraviolet produces cold H_2^+ , but hot H_2 . Modelling the wavepacket dynamics along the repulsive potential energy surface accounts for the repopulation of the ground potential energy surface. The role of the avoided crossing seam is emphasized and its importance for the astrophysically relevant charge transfer reactions is underlined.

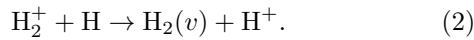
1. INTRODUCTION

The molecular ion H_3^+ plays a pivotal role in many astrophysical environments [1, 2]. In the interstellar medium, H_3^+ acts as a proton donor and provides the main path towards the formation of hydrides through the reaction $\text{H}_3^+ + \text{M} \rightarrow \text{H}_2 + \text{MH}^+$, which in turn leads to a sequence of ion-neutral reactions. H_3^+ is also a key species to understand deuterium fractionation: the main reservoir of deuterium is HD, which reacts with H_3^+ to form H_2D^+ . This leads to rapid deuteration at low temperature, as the reverse reaction is endothermic by 139.5 K. H_2D^+ then efficiently transfers its D in ion-neutral reactions, the differences in zero-point energy with respect to H-containing species leading to extreme deuteration at temperatures below 10-20 K.

The formation of H_3^+ in binary collisions of H_2 with H_2^+ is controlled by the ionization of H_2 . While cosmic rays are the main source of ionization in the interstellar medium, the reaction of vibrationally excited H_2 with protons is at play in hotter regions like shocked molecular clouds and the atmosphere of giant planets. Collision-induced vibrational excitation of H_2 triggers the charge transfer reaction:



In diffuse clouds where the density of H_2 is significantly lower than in dense clouds, the reverse reaction competes with the formation of H_3^+ from H_2^+ :

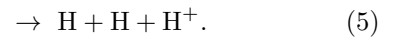
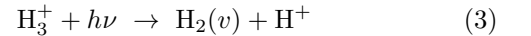


Both of these reactions are mediated by the H_3^+ potential energy surface. Numerous measurements of the cross section of reaction (1) exist, albeit with H_2 in its vibrational ground state and at collision energies well above 10 eV [3]. Our recent work on charge transfer in proton H_2 collisions down to 15 eV [4] demonstrated the decisive role

of the avoided crossing seam connecting the ground and first excited potential energy surfaces of H_3^+ . The vibrational population of the H_2^+ products was shown to peak at $v^+ = 0$ at a collision energy of 45 eV, evolving from a Franck-Condon distribution at keV energies. The current understanding is that the proton approach triggers the vibrational excitation necessary for the reaction (1) to proceed. This resonant population of $v^+ = 0$ vanishes at even lower energies.

The reverse reaction (2), despite its astrophysical importance, has received little attention. In their ion cyclotron resonance study at room temperature, Karpas *et al.* [5] determined the rate coefficient of all isotopic variants of the reaction, from which they could infer that the reaction does not proceed via scrambling nor via atom transfer, but rather via direct electron transfer. A merged beam study of the $\text{H} + \text{D}_2^+$ charge transfer reaction was performed by Andrianarijaona *et al.* [6] down to 1 eV, albeit with hot H_2^+ ions as produced by electron impact [7]. Finally, a detailed theoretical study was performed by Krstić [8], who predicts a vibrational distribution of H_2 products dominated by $v = 4$ down to ~ 1 eV, an energy below which all accessible levels become significantly populated.

While reactions (1) and (2) probe the crossing seam in a full collision, the photodissociation of H_3^+ is actually probing it from within, as fragments depart from the classical turning point accessed via a vertical transition from the ground state potential well. In this work, we consider the electronic excitation of the H_3^+ ground state to the first excited $^1A'$ state by UV photons of 4 to 5 eV, that triggers rapid dissociation into two or three products:



The case of infrared photodissociation of H_3^+ to $\text{H}_2 + \text{H}^+$ via quasi-bound resonances at the dissociation limit, as studied by Carrington and Kennedy [9], will not be discussed here, as it does not involve the first excited potential energy surface. The adiabatic dissociation limit

*Electronic address: xavier.urbain@uclouvain.be

of the $2^1A'$ state is $H_2^+ + H$, while the ground state dissociates to $H_2 + H^+$, the two limits being separate 1.83 eV in their respective vibrational ground states. Two-body channels $H_2 + H^+$ and $H_2^+ + H$ are situated 4.48 eV and 2.65 eV below the full atomisation limit respectively.

A decisive experiment should ideally discriminate between these different channels, measure the associated kinetic energy release and determine the vibrational distribution of the molecular products. Such an experimental effort will be described in the next sections. A quantum-chemical description of H_3^+ allowing for a complete determination of its potential energy landscape a time-dependent wavepacket simulation will be shown to give valuable insight into the non-adiabatic dynamics associated with the avoided crossing seam.

2. THE AVOIDED CROSSING SEAM

The potential energy surfaces of the H_3^+ molecular ion are known to exhibit a rich topology, which results from the high degree of symmetry imposed by the indistinguishability of the protons, and the asymptotic degeneracy of its fragmentation channels that stems from it. We shall discuss it here in terms of Jacobi coordinates r , R and θ . In the asymptotic region, r is the internal coordinate of a diatomic fragment, i.e. H_2 or H_2^+ , while R is the distance between the atomic fragment, i.e. H or H^+ , to the centre-of-mass of the diatom. Numerous calculations of the three-dimensional surfaces exist to this day [10, 11], that reveal the existence of an avoided crossing between the ground and first excited potential at distances $R \gtrsim 6 a_0$. When dealing with two-body breakup, the C_{2v} symmetry corresponding to $\theta = 90^\circ$, is usually preferred as it allows a simple representation of the surfaces. Its validity for the description of H_3^+ dynamics is expected to be somewhat limited, in view of the floppy character of the molecule above its barrier to linearity, located some $10,000 \text{ cm}^{-1}$ above its rovibrational ground state [12].

In their pioneering work, Preston and Tully [13] had performed a diatomics-in-molecules (DIM) calculation of the ground and first excited $^1A'$ potential energy surfaces of H_3^+ , revealing the avoided crossing seam resulting from the difference in dissociation energy between H_2 and H_2^+ exceeding that of ionization potential between H_2 and H . Bauschlicher *et al.* [14] have soon after performed the first *ab initio* calculation of those surfaces, and quantified the surface hopping probability at various R distances by reformulating the Landau-Zener-Stueckelberg transition probabilities in terms of adiabatic potentials. Their results were verified and expanded by Ichihara and Yokoyama [15] over the entire domain of Jacobi angle from 0° (collinear) to 90° (isosceles triangle).

In order to be able to run dynamical simulations, we have generated these potential energy surfaces in C_{2v} with the CASSCF + Full CI method as implemented in MOLPRO [16], the results of which are shown in figure 1.

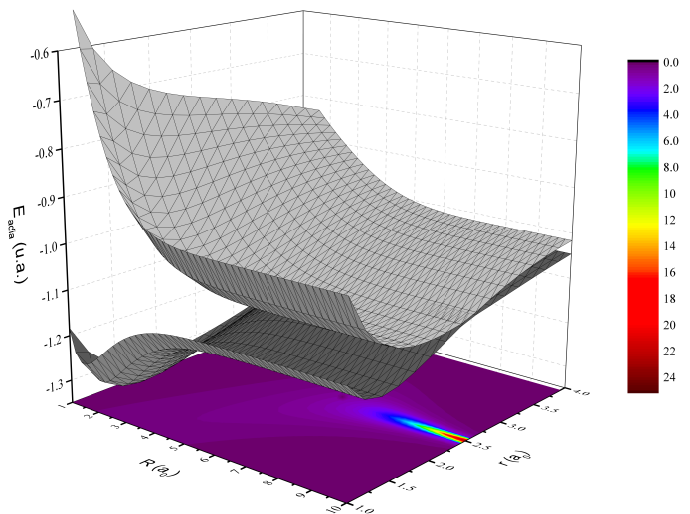


FIG. 1: Adiabatic potential energy surfaces of the two first 1A_1 states of H_3^+ . Colour map: non-adiabatic coupling matrix elements (a.u.) along r .

The energies were calculated on a grid of 150 points in r (from 0.6 to $38 a_0$ with additional points close to the crossing) and 69 points in R (from 1 to $20 a_0$) with a total of 10350 points. The basis set is AVTZ supplemented by additional functions, as employed for HeH^+ by Loreau *et al.* [17]. The non-adiabatic coupling matrix elements (NACME) were calculated on the same grid as the PES with the three-point method. Their value is represented in the colour map under the surface plot. The cusp corresponding to the avoided crossing appears at $r \simeq 2.5 a_0$ for distances R beyond $6 a_0$. The non-adiabatic coupling is in good agreement with previous calculations [18, 19].

3. ULTRAVIOLET PHOTODISSOCIATION OF H_3^+

Photodissociation, being essentially a half-collision process, offers a convenient probe of the long-range dynamics without the impact parameter averaging imposed by full collisions. In their seminal work on time-dependent wavepacket propagation, Kulander and Heller [20] have computed the photodissociation cross section for H_3^+ in its absolute ground state. The cross section was found to peak around 21 eV, rendering the photodissociation of H_3^+ in astrophysical environments rather unlikely [21]. The calculation included the first 1B_2 potential energy surface (in C_{2v} symmetry), which is degenerate with the 2^1A_1 at equilibrium geometry. While the dissociation along that third surface exclusively feeds the three-body channel $H + H + H^+$, the ground and first excited 1A_1 surfaces were treated in a diabatic picture, neglecting the interaction between them. The vibrational population of the H_2^+ products was found to peak at $v^+ = 0$, a result we shall put in perspective with our experimental findings.

Such photodissociation events were recorded by Bae and Cosby [22] in a fast beam experiment in collinear geometry where H_2^+ fragments were electrostatically separated and counted. Not surprisingly, the process was found to be absent at photon energies below 2.5 eV, while its yield increased steadily with photon energy above that. An apparent cross section as low as 10^{-22} cm² was measured at 4 eV, which is five orders of magnitude below the photodissociation cross section of H_2^+ .

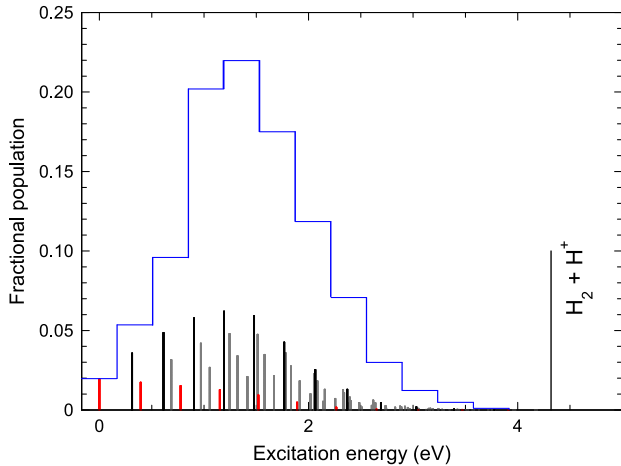
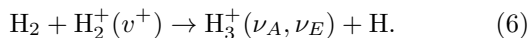


FIG. 2: Statistical population of (ν_A, ν_E) modes (red: $(\nu_A, 0)$ levels, black: $(0, \nu_E)$ levels, grey: combined excitations) following H_3^+ formation through reaction (6) from [23]. Histogram: binned excitation energy distribution.

This observation may be rationalised with the help of the internal energy distribution resulting from the H_3^+ formation process:



Anicich and Futrell [23] have calculated the population of the symmetric (ν_A) and doubly degenerate asymmetric (ν_E) mode for reaction (6) with the help of a statistical model accounting for the vibrational distribution of the H_2^+ reactant, as depicted in figure 2. One observes a tail in the distribution that extends towards the dissociation limit. Bae and Cosby however operated with a source consisting of a pulsed valve coupled with an electron gun, causing the nascent internal excitation to be substantially quenched during the expansion of the gas plume.

More recently, Alexander *et al.* [24] have observed the decay of the photodissociation signal in an ion beam trap. D_3^+ ions were produced in an electron cyclotron resonance source and stored between electrostatic mirrors. An intense femtosecond laser operating at 800 nm caused photodissociation of a decaying fraction of the stored ions as monitored by the detection of neutral particles leaving the trap. At such a long wavelength, the process is multiphotonic in nature, the molecular ions likely absorbing up to three photons at the highest intensities used in the experiment. More complete experiments were performed at 790 nm by Saylor *et al.* [25].

Petrignani *et al.* [26] have reported a similar experiment performed at the TSR ion storage ring in Heidelberg with a nanosecond laser of moderate intensity operating on the second and fourth harmonic of the Nd:YAG laser, i.e. 532 nm and 266 nm, respectively. In this single photon regime, the photodissociation signal, as observed by the detection of H_2^+ ions leaving the storage ring orbit, exhibit a rapid decay in the millisecond range, that was attributed to the depopulation of the tail of the distribution of internal states by radiative cooling. Complementary measurements were performed with a single-pass set-up in Louvain-la-Neuve, which will be described in some more detail below since new measurements have been performed to corroborate theoretical findings.

3.1. Experimental set-up

Our experimental setup is based on a small scale accelerator delivering beams of tens of nanoamperes at a few keV. The ions are created in a duoplasmatron source by electron impact ionization of H_2 and subsequent collisions, and should adopt an internal energy distribution similar to what was predicted by Anicich and Futrell [23] (figure 2). After acceleration, the beam is strongly collimated and crossed at right angle with the pulsed laser beam (figure 3) Experiments have been conducted at two different wavelengths, i.e. 300 nm and 266 nm. The former was produced by a dye laser pumped by the second harmonic of a nanosecond Nd:YAG laser (Continuum), while the latter is the fourth harmonic of the Nd:YAG obtained by frequency doubling the second harmonic output of the Nd:YAG integrated in our OPO laser system (Ekspla). Both lasers operate at a repetition rate of 30 Hz. The ion beam is chopped in 500 ns-long bunches synchronised to the laser shots in order to limit the load on the detectors located 1.75 m downstream. The primary H_3^+ ions are collected in a small Faraday cup located in front of the pair of detectors consisting of a Z-stack of microchannel plates backed with a resistive anode (Quantar).

The detectors are arranged as to minimize the dead area between them. To this goal, the second detector has been placed 10 cm downstream of the first one. This offers a second advantage: ions passing along the first detector's back plane get deflected sideways, allowing their easy separation from the neutrals impinging the second detector. The selection of a particular event is based on the successful reconstruction of its centre-of-mass both in time and position, i.e. the arrival time and location of the non-dissociated H_3^+ . Note however that this two-detector arrangement does not allow for the detection of the three-body breakup, reaction (5).

Since the vibrational excitation cannot be unequivocally determined from the measured kinetic energy release due to the unknown starting point in the H_3^+ potential well, one must rely on a post-interaction analysis of the products. The latter is performed by means of

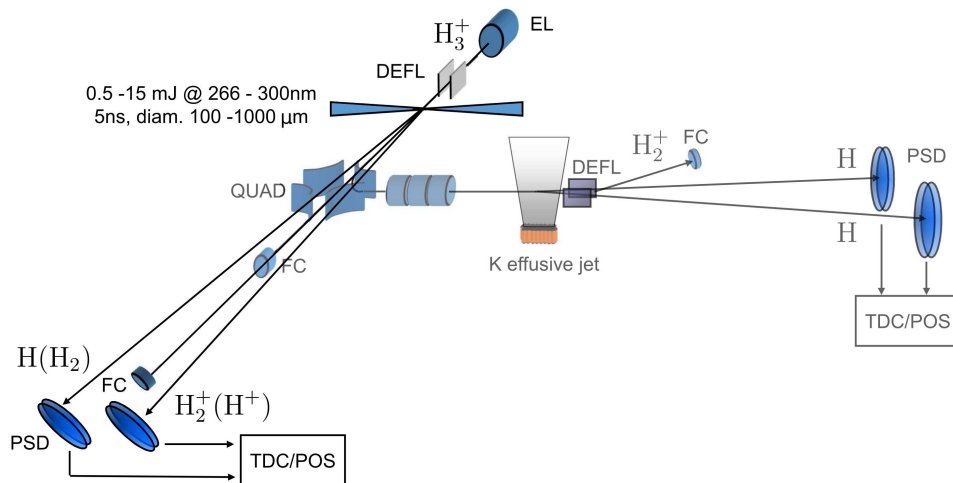


FIG. 3: Experimental set-up. EL: Einzel lens, DEFL: electrostatic deflector used as beam chopper, QUAD: quadrupole deflector, FC: Faraday cup, PSD: position-sensitive detectors, TDC: time-to-digital converter, POS: position analyser.

our dissociative charge transfer method as described in our study of the vibrational distribution of H_2^+ resulting from intense laser-field ionisation of H_2 [27]. In a nutshell, the molecular ions are deflected by an electrostatic quadrupole towards an effusive potassium jet, where they undergo resonant electron capture to the $a^3\Sigma_g^+$ and $c^3\Pi_u$ states of H_2 . The former quickly radiates to the repulsive $b^3\Sigma_u^+$ state while the latter is rotationally predissociated by the same b state, resulting in a pair of ground state atoms whose kinetic energy bears the imprint of the initial vibrational excitation [28]. A last complication arises from the fact that the molecular ions themselves have a kinetic energy that depends on the initial photodissociation event. Time-of-flight selection applied to the centre-of-mass of the two hydrogen atoms allows for a complete reconstruction of the stepwise fragmentation. Note that the same recipe does not apply to the vibrational analysis of H_2 products.

3.2. Experimental results

Kinetic energy release (KER) measurements have been performed under varying ion source conditions, and over a wide range of laser intensities, in order to investigate the role of initial excitation of the ions, and the possible occurrence of secondary photodissociation of the H_2^+ products. The KER distributions resulting from photodissociation of H_3^+ at 266 nm are shown in figure 4. Vibrational ladders are placed assuming the peak of the $\text{H}_2^+ + \text{H}$ distribution coincides with $v^+ = 0$, as discussed below.

Similar results were obtained at 300 nm, although the ground state channel (reaction (3)) was most often barely visible amongst the excessive collisional background present in our first set of experiments. In both cases, the distribution of $\text{H}_2^+ + \text{H}$ events (reaction (4))

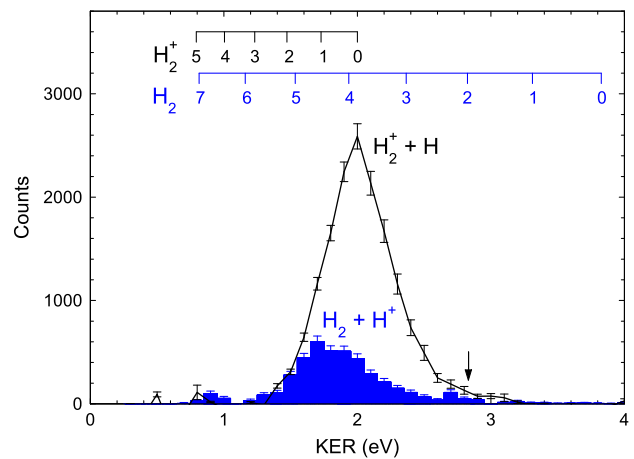


FIG. 4: Measured kinetic energy release distributions for the $\text{H}_2^+ + \text{H}$ and $\text{H}_2 + \text{H}^+$ channels. The arrow marks the expected KER for H_3^+ at the dissociation limit. Integrated counts reflect the actual branching ratio.

adopts a triangular shape, centred around 2 and 1.67 eV at 266 nm and 300 nm, respectively, while the ground state channel, $\text{H}_2 + \text{H}^+$, peaks at slightly lower energy, i.e. 1.75 eV at 266 nm. The branching ratio is about 4:1 in favour of the $\text{H}_2^+ + \text{H}$ channel (see table I), confirming the intervention of the crossing seam in the dissociation dynamics.

Our KER spectra are remarkably similar to the measurements of Gaire *et al.* [29] performed with 40 fs pulses at 395 nm. They also observed a 0.25 eV shift of the $\text{D}_2 + \text{D}^+$ peak towards lower energy, and a branching ratio of about 6:1 between the two channels. Considering the high intensity involved ($10^{14} \text{ W cm}^{-2}$), they assigned the $\text{D}_2 + \text{D}^+$ and $\text{D}_2^+ + \text{D}$ contributions to 2- and 3-photon processes, respectively. The present results challenge this interpretation.

TABLE I: Fractional population (in percent) of vibrational levels of H_2^+ measured at $\lambda = 266$ and 300 nm (exp). Two-dimensional wavepacket calculations at 58 nm (Kulander and Heller [20]), 266 nm and 300 nm (WP, present work). Vibrational distribution of H_2 from present wavepacket calculations. BF: branching fraction to $\text{H}_2^+ + \text{H}$ or $\text{H}_2 + \text{H}^+$.

v	58 nm		266 nm		300 nm		
	H_2^+ [20]	H_2^+ (exp)	H_2^+ (WP)	H_2 (WP)	H_2^+ (exp)	H_2^+ (WP)	H_2 (WP)
0	75	72(4)	88.0	0.0	63(5)	89.9	0.0
1	19	20(4)	3.1	0.0	23(5)	1.6	0.0
2	1.5	6(4)	5.6	0.0	13(5)	6.0	0.3
3	2.5	2(4)	3.0	1.9	1(5)	2.2	1.2
4	1.6		0.3	48.7		0.3	55.5
5	0.4		0.1	46.1		0.0	41.5
6	0.0			3.2			1.5
7				0.0			0.0
BF	100	79(4)	70.9	29.1	87(7)	71.5	28.5

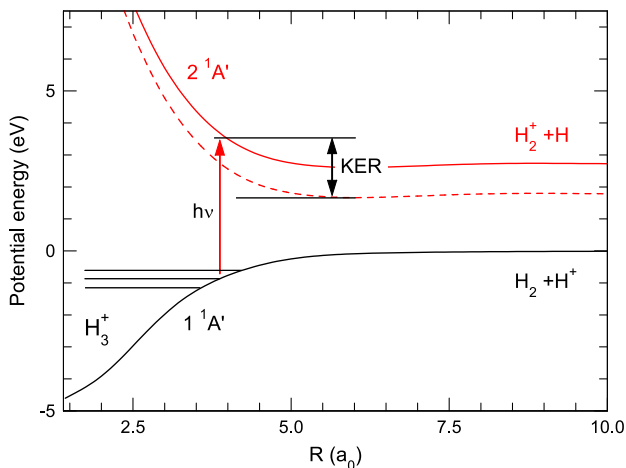


FIG. 5: Schematic representation of the UV excitation from the $1\ ^1A'$ to the $2\ ^1A'$ state. Full (dashed) lines are cuts through the potential energy surfaces at the equilibrium distance of H_2 (H_2^+). The actual kinetic energy release depends on the vibrational excitation of the H_2^+ product.

In order to confirm the dominant population of $v^+ = 0$, we also measured the vibrational distribution of emerging H_2^+ ions by means of our dissociative charge transfer method. For that purpose, the intensity of the H_3^+ beam had to be increased to hundreds of nA, as the combined charge transfer and coincidence detection efficiency does not exceed 10^{-3} . The analysis of the vibrational distributions is summarised in table I. More than two thirds of the population is concentrated in the $v^+ = 0$ level, while no population could be detected beyond $v^+ = 3$. This finding matches astonishingly well the theoretical prediction of Kulander and Heller [20], which is quite surprising when considering that they computed the distribution for cold H_3^+ while we measured with fairly hot ions. Moreover, their calculation deliberately ignored the presence of the avoided crossing seam, which is likely to contribute to ground state dissociation.

Building on this knowledge, one may locate the energy levels contributing the most to the photodissociation signal by subtracting the KER and the energy difference between the $\text{H}_2^+ + \text{H}$ and $\text{H}_2 + \text{H}^+$ asymptotes to the photon energy, as depicted in figure 5. These levels would sit 0.83 eV and 0.6 eV below the H_3^+ dissociation limit, at 266 nm and 300 nm respectively, which according to the work of Anicich and Futrell [23], constitute $\sim 0.5\%$ of the nascent vibrational distribution (see fig. 2). This tiny population is compatible with the apparent photodissociation cross section measured at 266 nm by Petrigiani *et al.* [26], i.e. $\sim 7 \times 10^{-20}$ cm².

3.3. Wavepacket simulations

In order to interpret these experimental observations, we performed time-dependent wavepacket calculations on the first two coupled potential energy surfaces. The time-dependent approach relies on the projection of the initial rovibrational wavefunction on the upper surface, after multiplication by the dipole matrix element. A more complete description of the photodissociation would in principle require to include the second excited singlet potential energy surface, which presents a conical intersection with the first excited potential in equilateral configurations [10]. However, our simulations show that at the wavelengths explored here, the wave packet does not reach this region.

As shown in figure 2, many vibrational states of H_3^+ are populated in the experiment. To identify the geometry where the initial wavepacket is defined on the excited potential energy surface, one may use the information provided by the KER and follow the principle illustrated by figure 5: the vertical transition from the ground to the first excited $1\ ^1A'$ surface must occur along a path corresponding to the so-called Condon point, where the potential energy difference matches the photon energy. Such contour lines are represented on figure 6 in C_{2v} symmetry for photon energies ranging from 2 to 10 eV. The loca-

tion of these transition points on the upper surface for the photon energies in the present experiment (4.133 eV or 4.661 eV) spans a wide energy domain (see figure 1), which in turn would generate a broad kinetic energy distribution, as shown by our experimental results (figure 4). Added in bold on figure 6 are the regions contributing to the peak of the KER distribution when considering $\text{H}_2^+(v^+ = 0)$ products only.

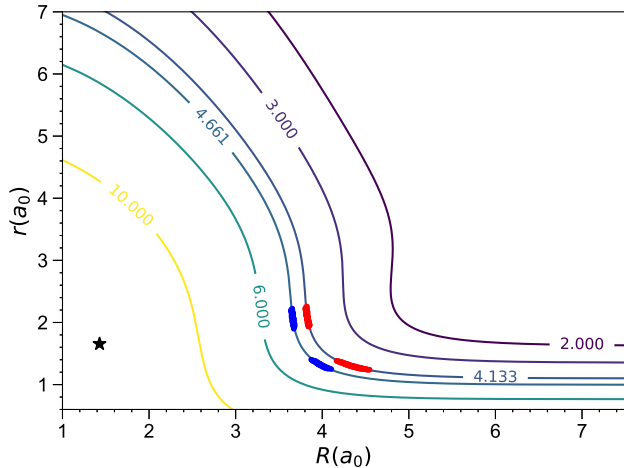


FIG. 6: Contour lines marking the region where the separation between the ground and first excited potential energy surfaces matches the indicated photon energies. The most likely transition regions at 266 nm (4.661 eV, blue) and 300 nm (4.133 eV, red) are marked by bold lines. The star marks the equilibrium geometry of H_3^+ .

To assess the role of the avoided crossing seam, time-dependent wavepackets were propagated on diabatic surfaces derived from our adiabatic potential energy surfaces and NACME (figure 1). A strict diabatisation was performed along the r coordinate with R fixed, since the avoided crossing is along the r coordinate. The two-dimensional wavepacket propagation was performed with the computer package WAVEPACKET of Schmidt and Lorenz [30]. Gaussian wavepackets were launched from a selection of starting coordinates (marked in bold on figure 6). Their vibrational analysis follows the method of Balint-Kurti *et al.* [31]. The Fourier transform of the wavepacket $\Phi(R, r, t)$ is computed at sufficiently large R_∞ and projected onto the vibrational wavefunctions $\chi_v(r)$ of the diatomic (H_2 or H_2^+):

$$A_v(R_\infty, E) = \frac{1}{2\pi} \int_0^\infty \exp(iEt/\hbar) \langle \chi_v(r) | \Phi(R_\infty, r, t) \rangle dt. \quad (7)$$

The square of the A_v amplitude is identified as the population of vibrational level v . The choice of the total energy E is somewhat arbitrary as several H_3^+ levels may contribute to the photodissociation signal at a given wavelength. For consistency, it is taken equal to the potential energy of the 2^1A_1 state at the initial position of the wavepacket.

The vibrational populations obtained when launching the wavepacket at ($R = 3.67 a_0, r = 2 a_0$) for 266 nm and ($R = 3.8 a_0, r = 2 a_0$) for 300 nm are given in table I. Both vibrational distributions are in fair agreement with experiment, with the H_2^+ population peaking at $v^+ = 0$ while the H_2 population is concentrated in $v = 4$ and 5, as suggested by the vibrational ladder in figure 4. Moreover, the computed branching ratio 0.71:0.29, is not too distant from the experimental values. Wave packet simulations were performed for initial geometries close to those reported above, indicated in Fig. 6, with qualitatively similar conclusions regarding the distribution of final vibrational states.

While these encouraging results confirm our interpretation, the initial state of H_3^+ is still ill-defined, borrowing from our knowledge of the average kinetic energy release. Specific rovibrational wavefunctions should in principle serve as an input, which is beyond the applicability of our model due to its reduced dimensionality. Obviously, a multidimensional treatment of the non-adiabatic interactions is also in order, as was recently performed by Alijah *et al.* [32] and Mukherjee *et al.* [33]. Such a full-dimensional quantum mechanical treatment was reported by Sun *et al.* [34]. While the authors present a kinetic energy spectrum for the photodissociation of H_3^+ at 266 nm, no mention is made of the avoided crossing seam, which is somewhat surprising considering the amount of computational effort.

4. CONCLUSION

We have carried out an experimental study of the UV photodissociation of H_3^+ towards $\text{H}_2 + \text{H}^+$ and $\text{H}_2^+ + \text{H}$ channels at wavelengths of 266 nm and 300 nm. Such wavelengths mainly probe the photodissociation from excited vibrational states of H_3^+ that are populated following its formation in the ion source plasma. The photodissociation is known to proceed through two potential energy surfaces that are connected by a seam of non-adiabatic couplings. While this seam plays a minor role in the photodissociation from the ground vibrational state of H_3^+ , the present measurements indicate that this is not the case for vibrationally excited ions. An analysis of the kinetic energy release of both channels was performed, showing a dominant contribution from the $\text{H}_2^+ + \text{H}$ channel with H_2^+ in the ground vibrational state. On the other hand, for the H_2 fragments a strong vibrational excitation was observed. These findings were rationalised by performing time-dependent wavepacket simulations of the photodissociation process, demonstrating the impact of the non-adiabatic seam on the dynamics. While the theoretical model was limited by considering only two reaction coordinates as well as by the uncertainty on the initial vibrational distribution of H_3^+ , it nevertheless provided a clear qualitative interpretation of the experimental results.

A natural extension of the present work would be to

include the 1B_2 potential energy surface that is degenerate with the $2\ {}^1A_1$ in equilateral triangle geometry. More importantly, one must consider different values of the Jacobi angle, since the latter was shown to be a crucial parameter controlling the vibrational excitation of H_2 in reaction (1) [35].

The photodissociation may not be of immediate astrophysical relevance, as it is listed in UMIST and other astrophysical databases with a negligible rate of $5 \times 10^{-15} s^{-1}$. This is solely due to the absorption window being located around 21 eV. Assuming there are environments where vibrationally excited H_3^+ are exposed to VUV radiation, a moderate vibrational excitation could already lead to a substantial shift of the absorption window towards longer wavelengths due to the steepness of the upper potential energy surface.

The knowledge gathered in the present study is readily transposable to the charge transfer reactions (2) and (1), as they share the same avoided crossing seam dynamics. In that respect, the study of photodissociation at longer wavelength would give access to vibrational states of large deformation as predicted to exist close to the

dissociation threshold [36]. Such studies will serve as an additional benchmark of the existing surfaces and non-adiabatic coupling matrix elements.

Acknowledgments

The authors thank H. Kreckel for fruitful discussions. They are indebted to J. Liévin for having suggested to investigate the role of the crossing seam motivating the present study.

This work was supported by the Fonds de la Recherche Scientifique-FNRS through IISN grant No. 4.4504.10. Computational resources have been provided by the Consortium des équipements de Calcul Intensif (CÉCI), funded by the Fonds de la Recherche Scientifique-FNRS under Grant No. 2.5020.11. The authors thank the Belgian State for the grant allocated by Royal Decree for research in the domain of controlled nuclear fusion. XU is Senior Research Associate of the Fonds de la Recherche Scientifique-FNRS.

-
- [1] J. Tennyson, *Rep. Prog. Phys.* **58**, 421 (1995).
 [2] T. Oka *Chem. Rev.* **113**, 8738 (2013).
 [3] Kusakabe T, Pichl L, Buenker RJ, Kimura M, Tawara H 2004 Isotope effect in charge-transfer collisions of slow H^+ and D^+ ions with H_2 , HD, and D_2 molecules *Phys. Rev. A* **70** 052710.
 [4] Urbain X, de Ruelle N, Andrianarijaona VM, Martin MF, Fernández Menchero L, Errea L, Méndez L, Rabadán I, Pons B 2013 New Light Shed on Charge Transfer in Fundamental $H^+ + H_2$ Collisions *Phys. Rev. Lett.* **111** 203201.
 [5] Karpas Z, Anicich V, Huntress Jr WT 1979 An ion cyclotron resonance study of reactions of ions with hydrogen atoms *J. Chem. Phys.* **70** 2877-2881.
 [6] Andrianarijaona VM, Rada JJ, Rejoub R, Havener CC 2009 Investigation of charge transfer in low energy $D_2^+ + H$ collisions using merged beams *J. Phys. Conf. Ser.* **194** 012043.
 [7] von Busch F, Dunn GH 1972 Photodissociation of H_2^+ and D_2^+ : Experiment *Phys. Rev. A* **5** 1726.
 [8] Krstić PS 2002 Inelastic processes from vibrationally excited states in slow $H^+ + H_2$ and $H + H_2^+$ collisions: Excitations and charge transfer *Phys. Rev. A* **66** 042717.
 [9] Carrington A, Kennedy RA 1984 Infrared predissociation spectrum of the H_3^+ ion *J. Chem. Phys.* **81** 91-112.
 [10] Viegas LP, Alijah A, Varandas AJ 2007 Accurate ab initio based multisheeted double many-body expansion potential energy surface for the three lowest electronic singlet states of H_3^+ *J. Chem. Phys.* **126** 074309, and references therein.
 [11] Pavanello M, Adamowicz L, Alijah A, Zobov NF, Mizus II, Polyansky OL, Tennyson J, Szidarovszky T, Császár AG 2012 Calibration-quality adiabatic potential energy surfaces for H_3^+ and its isotopologues *J. Chem. Phys.* **136** 184303.
 [12] Röhse R, Kutzelnigg W, Jaquet R, Klopper W 1994 Potential energy surface of H_3^+ ground state in the neighborhood of the minimum with micro-Hartree accuracy vibrational frequencies derived from it *J. Chem. Phys.* **101** 2231-2243.
 [13] Preston RK, Tully JC 1971 Effects of surface crossing in chemical reactions: the H_3^+ system *J. Chem. Phys.* **54** 4297-4304.
 [14] Bauschlicher Jr CW, O'Neil SV, Preston RK, Schaefer III HF, Bender CF 1973 Avoided intersection of potential energy surfaces: The ($H^+ + H_2$, $H + H_2^+$) system *J. Chem. Phys.* **59** 1286-1292.
 [15] Ichihara A, Yokoyama K 1995 Ab initio potential energy surfaces for the two lowest ${}^1A'$ states of H_3^+ *J. Chem. Phys.* **103** 2109-2112.
 [16] Werner HJ, Knowles PJ, Knizia G, Manby FR, Schütz M, et al. 2012 MOLPRO: a general-purpose quantum chemistry program package.
 [17] Loreau J, Liévin J, Palmeri P, Quinet P, Vaecq N 2010 Ab initio calculation of the 66 low-lying electronic states of HeH^+ : adiabatic and diabatic representations *J. Phys. B: At. Mol. Opt. Phys.* **43** 065101.
 [18] Barragán P, Errea LF, Macías A, Méndez L, Rabadán I, Riera A, Lucas JM, Aguilar A 2004 Study of ab initio molecular data for inelastic and reactive collisions involving the H_3^+ quasimolecule *J. Chem. Phys.* **121** 11629.
 [19] Barragán P, Errea LF, Macías A, Méndez L, Rabadán I, Riera A 2006 A study of conical intersections for the H_3^+ system *J. Chem. Phys.* **124** 184303.
 [20] Kulander KC, Heller EJ 1978 Time dependent formulation of polyatomic photofragmentation: Application to H_3^+ *J. Chem. Phys.* **69** 2439-2449.
 [21] van Dishoeck EF 1987 Photodissociation processes of astrophysical molecules. In *Symposium-International Astronomical Union* **120** 51-65, Cambridge University

- Press.
- [22] Bae YK, Cosby PC 1990 Observation of bound-free photodissociation of H_3^+ *Phys. Rev. A* **41** 1741.
- [23] Anicich VG, Futrell JH 1984 A computer study of the formation of H_3^+ and its vibrational deactivation using a statistical model *International journal of mass spectrometry and ion processes* **55** 189-215.
- [24] Alexander JD, Calvert CR, King RB, Kelly O, Graham L, Bryan WA, Nemeth GRAJ, Newell WR, Froud CA, Turcu ICE, Springate E, Williams ID, Greenwood JB 2009 Photodissociation of D_3^+ in an intense, femtosecond laser field *J. Phys. B: At. Mol. Opt. Phys.* **42** 141004.
- [25] Sayler AM, McKenna J, Gaire B, Kling NG, Carnes KD, Ben-Itzhak I 2012 Measurements of intense ultrafast laser-driven D_3^+ fragmentation dynamics *Phys. Rev. A* **86** 033425.
- [26] Petrigiani A, Bing D, Novotny O, Berg MH, Buhr H, Grieser M, Jordon-Thaden B, Krantz C, Mendes MB, Menk S, Novotny S, Orlov DA, Repnow R, Stützel J, Urbain X and Wolf A 2010 Ultraviolet and Visible Light Photodissociation of H_3^+ in an Ion Storage Ring *J. Phys. Chem. A* **114** 4864-4869.
- [27] Urbain X, Fabre B, Staicu-Casagrande EM, de Ruelle N, Andrianarijaona VM, Jureta J, Posthumus JH, Saenz A, Baldit E, Cornaggia C 2004 Intense-laser-field ionization of molecular hydrogen in the tunneling regime and its effect on the vibrational excitation of H_2^+ *Phys. Rev. Lett.* **92** 163004.
- [28] De Bruijn DP, Neuteboom J, Los J 1984 Predissociation of the $c^3\Pi_u$ state of H_2 , populated after charge exchange of H_2^+ with several targets at keV energies *Chem. Phys.* **85** 233-251.
- [29] Gaire B, McKenna J, Zohrabi M, Carnes KD, Esry BD, Ben-Itzhak I 2012 Dynamics of D_3^+ slow dissociation induced by intense ultrashort laser pulses *Phys. Rev. A* **85** 023419.
- [30] Schmidt B, Lorenz U 2017 WavePacket: A Matlab package for numerical quantum dynamics. I: Closed quantum systems and discrete variable representations *Comput. Phys. Comm.* **213** 223-234.
- [31] Balint-Kurti GG, Dixon RN, Marston CC 1990 Time-dependent quantum dynamics of molecular photofragmentation processes. *J. Chem. Soc. Faraday Trans.* **86** 1741-1749.
- [32] Alijah A, Fremont J, Tyuterev VG 2015 Quantized non-adiabatic coupling terms of H_3^+ *Phys. Rev. A* **92** 012704.
- [33] Mukherjee B, Mukherjee S, Adhikari S 2016 Ab-initio non-adiabatic couplings among three lowest singlet states of H_3^+ : Construction of multisheeted diabatic potential energy surfaces *Journal of Physics: Conference Series* **759** 012050.
- [34] Sun Z, Yang C, Zheng Y 2015 Laser-induced dissociation dynamics of triatomic molecule in electronic excited states: A full-dimensional quantum mechanics study *J. Chem. Phys.* **143** 224309.
- [35] Errea LF, Fernández L, Méndez L, Pons B, Rabadán I, Riera A 2007 Vibronic treatment of vibrational excitation and electron capture in $H^+ + H_2$ (HD, D_2) collisions at low impact energies *Phys. Rev. A* **75** 032703.
- [36] Munro JJ, Ramanlal J, Tennyson J 2005 Asymptotic vibrational states of the H_3^+ molecular ion *New J. Phys.* **7** 196.